Material: Ferritic Steel: F82H
Property: crack length (mm) versus stress intensity factor (MPa*sqrt(m))
Condition: none
Data: Experimental

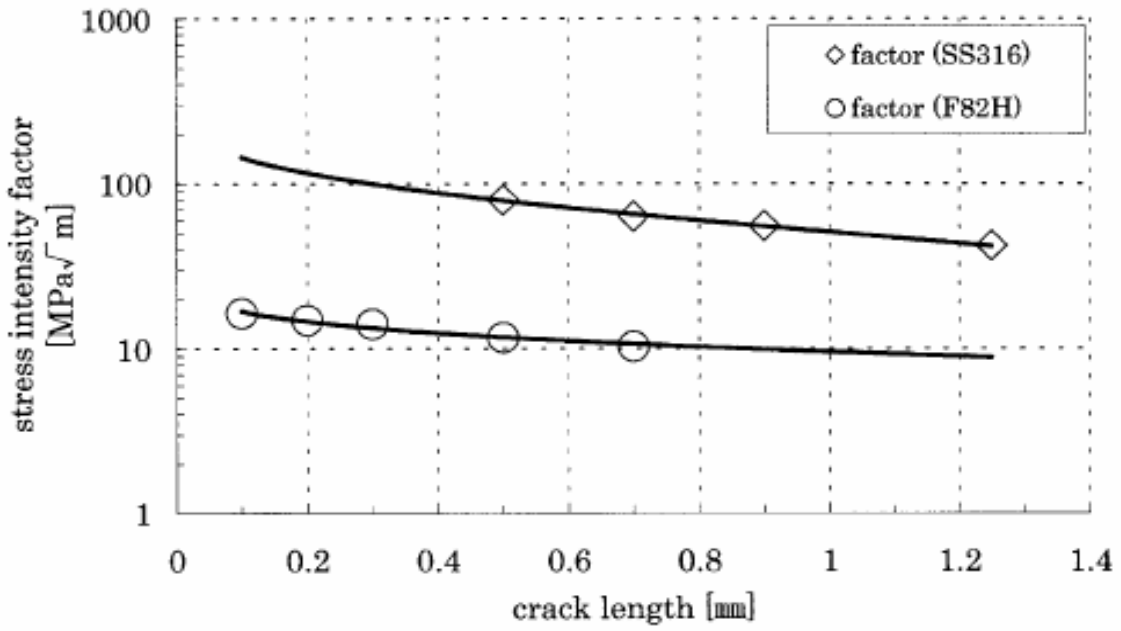

Fig. 7. Stress intensity range against crack length.

Source:
Journal of Nuclear Materials, 307-311, 2002, 471-474

Title of paper (or report) this figure appeared in:
Thermal fatigue crack propagation behavior of F82H ferritic steel

Author of paper or graph:
Yusuke Kudo, Kouichi Kikuchi, Masakatsu Saito

Caption:
Stress intensity range against crack length.

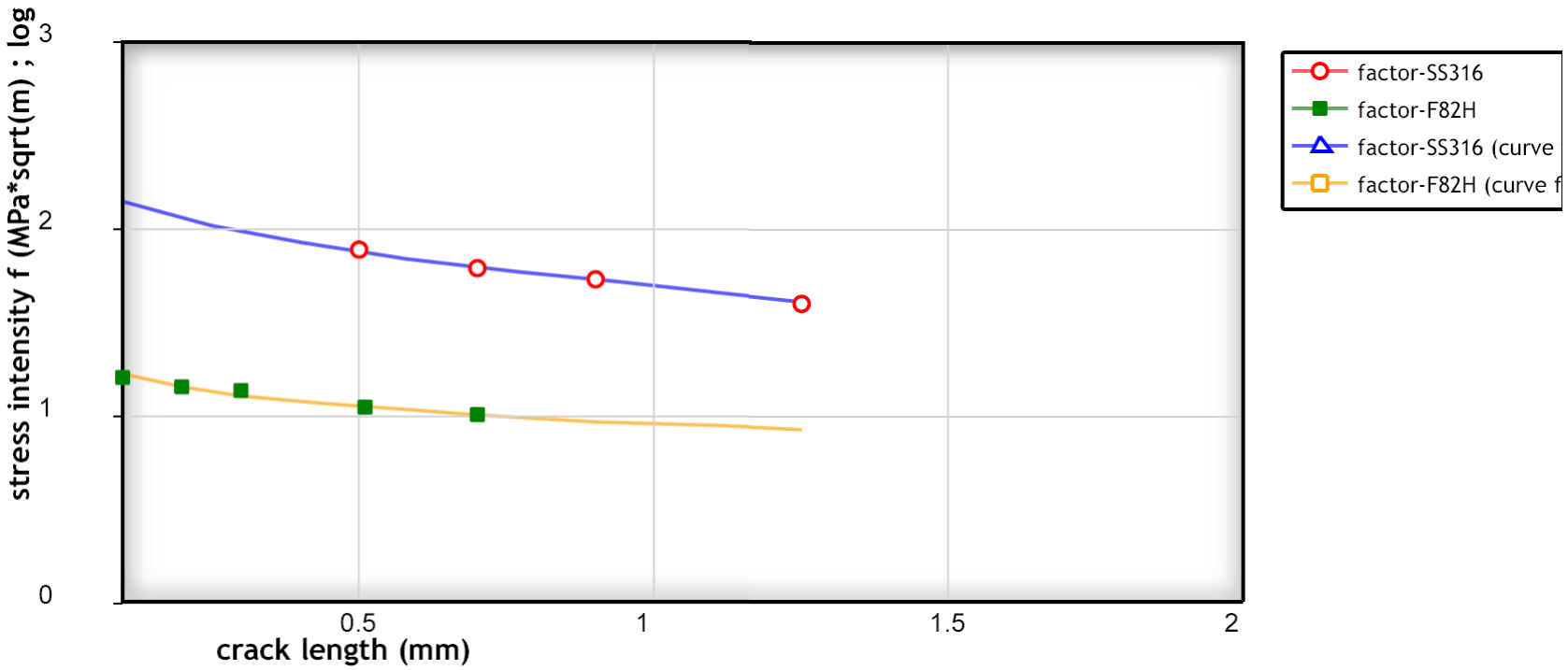

Stress intensity range against crack length.

Reference:

Author: *Yusuke Kudo, Kouichi Kikuchi, Masakatsu Saito*
Title: *Thermal fatigue crack propagation behavior of F82H ferritic steel*
Source: *Journal of Nuclear Materials, 2002, Volume 307-311, Page 471-474*, [PDF]

View Data | Author Comments

Plot Format:

Y-Scale: ○ linear ◉ log ○ ln
X-Scale: ◉ linear ○ log ○ ln

Update | Close Window

ELSEVIER

Journal of Nuclear Materials 307–311 (2002) 471–474

journal of nuclear materials

www.elsevier.com/locate/jnucmat

Thermal fatigue crack propagation behaviour of F82H ferritic steel

Yusuke Kudo [a,*], Kouichi Kikuchi [b], Masakatsu Saito [c]

[a] *Naka Fusion Research Establishment, Japan Atomic Energy Research Institute, Mukouyama, Naka-machi, Naka-gun, Ibaraki-ken, 311-0193 Japan*

[b] *Mitsubishi Heavy Industries, Kobe, 652-8585 Japan*

[c] *Institute of Engineering Mechanics, University of Tsukuba, Ibaraki, 305-8573 Japan*

Abstract

This paper presents an issue obtained from thermal fatigue research, which attempts to examine the fusion reactor first wall by fracture mechanics. The research is organised with two different approaches: 1. Studies of the thermal fatigue crack propagation behaviour on notched 5-mm thick plate specimens of ferritic steel F82H (9Cr-1W), compared with 9Cr-1Mo ferritic steel and type 316 stainless steel; 2. Numerical simulations of the stress field caused by thermal loads including fracture mechanics. It is concluded that the stress intensity factor ΔK_I is substantial for crack growth while cyclic thermal loading.

1. Introduction

The fusion reactor first wall is subjected to high cyclic temperature changes, which causes temperature gradients across the wall thickness and thermal stresses due to large structure constraints. However, the bending deformation is almost restricted. During plasma operation, the plasma side is exposed to compressive and the coolant side to tensile thermal stresses. The existence of initial defects or operational flaw inside the first wall is possible; hence compressive stress intensity occurs near the vicinity of defects during the plasma operation and plastic deformation is induced. At the end of each operational term, the temperature within the first wall decreases and tensile residual stresses results from the surrounding elastic zone of the crack tip. These sequential stress fluctuations promote crack growth.

This report describes the thermal fatigue crack propagation behaviour of F82H. The thermal fatigue experiments by electron beam as a heat flux source were carried out on 5-mm thick specimens. In comparison with F82H, 9Cr-1Mo ferritic steel, the commercial grade of F82H and type 316 stainless steel (SS316) were also examined. The difference between the two ferritic steels is the concentration of critical alloying elements of F82H, which was lower in case of the commercial grade ferritic steel to achieve low radiation activation [1]. On the other hand, the thermal and residual stress fields around the crack tip were analysed numerically. The three-dimensional finite element code 'MARC' was used to simulate the stress strain field during thermal fatigue experiment.

Previous thermal fatigue research on stainless steel described the crack propagation behaviour by using COD or ΔJ value [2,3]. In this paper, the stress intensity factor is introduced to explain this behaviour.

2. Experiment description

The mechanical properties of the materials used in these experiments are shown in Table 1 [1]. The dimensions of the specimen are displayed in Fig. 1. The 5-mm thick specimen was notched at the centre by electro spark machining to propagate the initial crack. A 0.1 mm

* Corresponding author. Tel: +81-29 270 7431; fax: +81-29 270 7449.

E-mail address: kudou@fusion.naka.jaeri.go.jp (Y. Kudo).

0022-3115/02/$ - see front matter
PII: S0022-3115(02)01038-3

Table 1
Mechanical properties at 293 K

Material	0.2% proof strength (MPa)	Tensile strength (MPa)	Elongation (%)
F82H	461	607	25
SS316	255	604	55
9Cr-1Mo	270	510	40

deep pre-crack was initiated by cyclic mechanical fatigue. The length of the pre-crack was empirically calibrated by measuring the cyclic dependency on the mechanical fatigue crack length. Temperature histories at the point T1 were measured with a radiation thermometer and at T2 with a thermocouple and to observe the experimental condition for the numerical simulations. The apparatus, as shown schematically in Fig. 2, consists of a vacuum chamber and a servo-hydraulic fatigue-testing machine. The specimen was clamped between two pistons, to restrict bending deformation and to allow only longitudinal movement. An ambient temperature water-cooled copper block was also attached to the specimen.

Once the specimen was positioned in the apparatus, it was subjected to cycles of 30 s duration consisting of heating for 5 s and cooling for 25 s. The centre of the specimen was irradiated by an electron beam and cooled

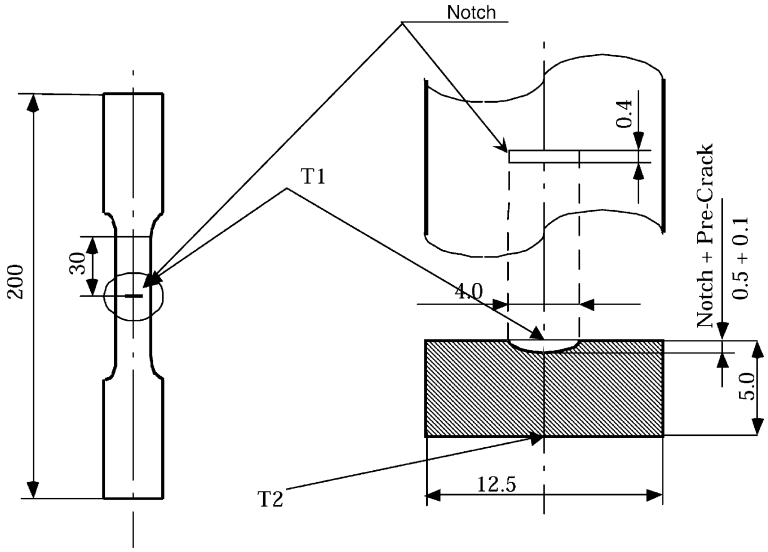

Fig. 1. Specimen size and measurement [mm].

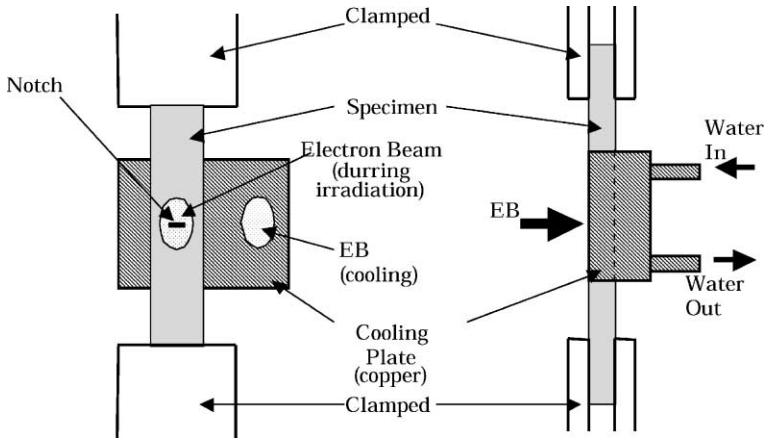

Fig. 2. Specimen in apparatus.

by diverting the electron beam to the cooling plate. The thermal loading was limited to a maximum surface temperature of 973 K; the distribution pattern of the heat flux on the surface was almost elliptic with diameters of 9.0 mm in vertical and 6.0 mm in horizontal direction. This resulted in power densities of 11 MW/m^2 for F82H and 9Cr-1Mo and 6 MW/m^2 for SS316.

The length of the thermal fatigue crack was measured along the specimen thickness direction from the bottom of the notch to the crack tip by using an optical microscope.

3. Analytical procedure

3.1. Analytical modelling

One fourth of the specimens was simulated by numerical analysis, as shown in Fig. 3. The coordinates of the analysis were adopted as: X-direction is parallel to the width, Y-direction is parallel to the thickness and Z-direction is parallel to the longitudinal axis of the specimen.

The thermal stress analysis consisted of two steps: transient heat transfer and thermal elasto-plastic stress calculation [4].

Like in case of the transient heat transfer analysis, the distribution of the measured heat flux was approximated with the Gaussian distribution for the numerical input. Temperature dependencies of thermal conductivity and specific heat were taken into account. The heat transfer coefficient between the cooling board and the specimen was hardly measured experimentally before. For this study the coefficient was derived from the comparison of temperature histories of experimental and simulated values. The numerical trials for the heat transfer coefficient were performed until both values tallied.

The temperature distribution from the transient heat transfer analysis was included in the thermal elasto-plastic stress simulations. The following boundary conditions were taken into consideration: the displacement in X-direction was fixed in the symmetric plane including the Y-axis; the displacement in Y-direction was fixed on the back surface attached to the cooling plate; the displacement in Z-direction was fixed in the plane including the crack. Temperature dependencies of the mechanical properties, such as the yield stress, Young modulus, Poisson ratio and the coefficient of the thermal expansion, were also taken into account [1].

3.2. Fracture mechanics method

A stress field due to thermal loading was evaluated by the linear fracture mechanics parameter, the stress intensity factor K [5]. The numerical simulations provided the principal stresses in the crack tip as tensile stresses. Therefore, K_I was introduced as governing parameter for crack propagation. K_I was derived by the extrapolation method. The fatigue crack propagation behaviour was determined with the stress intensity range of tensile stress fields, ΔK_I, and the crack length, where ΔK_I is given as:

$$\Delta K_I = K_{I\max} - K_{I\min} \quad \text{where } K_{I\min} < 0, \quad \text{then } K_{I\min} = 0.$$

It is assumed that the negative value of K_I does not contribute to crack propagation.

4. Results and discussion

The results of the conducted thermal fatigue tests are shown in Fig. 4. The crack length in case of F82H does not even reach half of the specimen thickness after 10000 cycles. On the other hand, the crack in SS316 propagates more than half of its thickness after 5000 cycles regardless the reduced heat load compared to F82H.

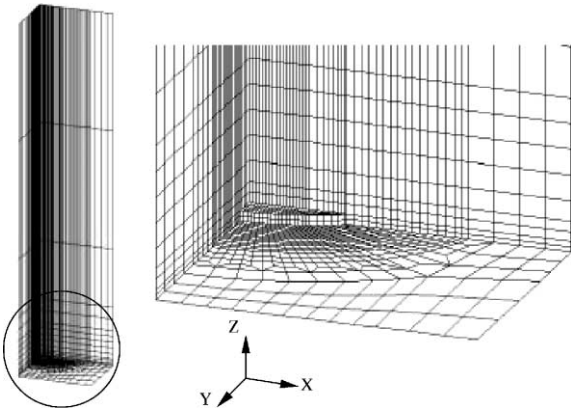

Fig. 3. Numerical analysis model.

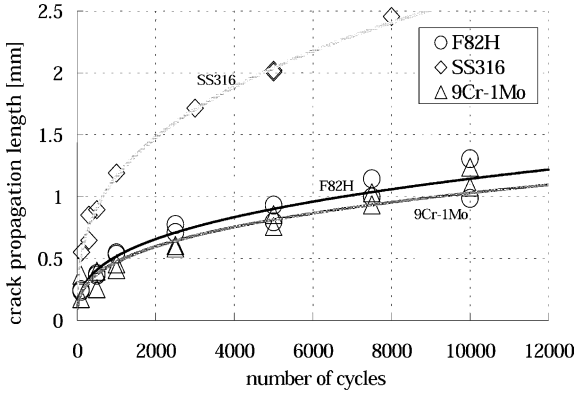

Fig. 4. Crack propagation length against the number of cycles.

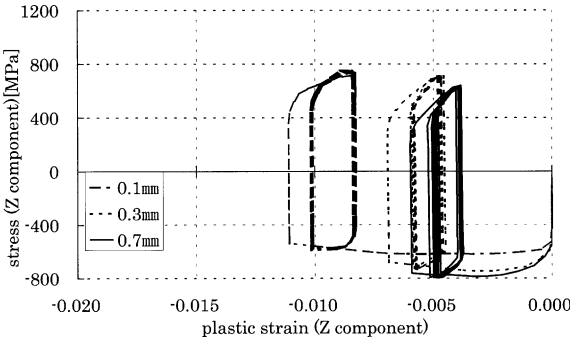

Fig. 5. Stress–plastic strain curve (F82H).

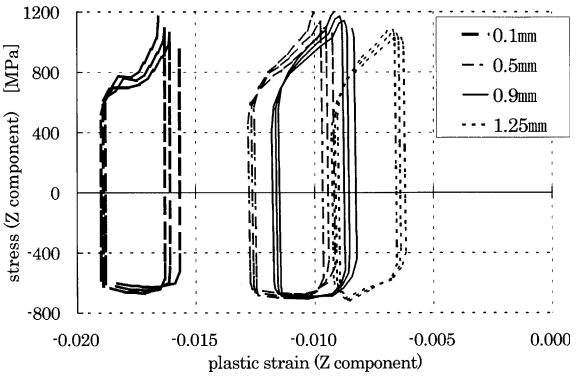

Fig. 6. Stress–plastic strain curve (SS316).

There is no difference in crack propagation between 9Cr-1Mo ferritic steel and F82H.

Figs. 5 and 6 show the converged hysteresis loops corresponding to each crack length of F82H and SS316 respectively. The area of each loop decreases as the crack length increases. This indicates that the dissipating energy from cyclic thermal loading decreases, because the stress intensity is released by the crack growth and also the cooling down promotes the recovery of material properties. The converged hysteresis loops of F82H are narrower compared to SS316 regardless of higher yield stress. Numerical results show hardly any crack propagation in case of F82H. Hence, the thermal stresses are much higher for SS316, which agrees with experimental results.

Fig. 7 shows the range of the stress intensity factor of each material as a function of the crack length. The stress intensity ranges of the tensile stress filed for the two samples are different, the stress intensity range of F82H is one seventh of SS316. The comparison of these stress fields around the crack tip indicates the superiority of F82H to SS316 in thermal fatigue behaviour.

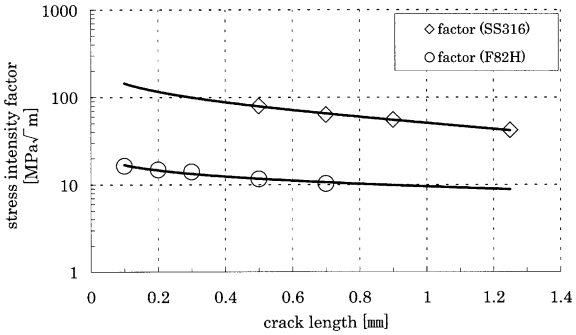

Fig. 7. Stress intensity range against crack length.

5. Concluding remarks

Pulsed heat flux irradiation tests were performed on F82H, 9Cr-1Mo ferritic steel and SS316 to investigate the thermal fatigue behaviour in experimental as well as analytical approaches. Conclusions that can be drawn from this investigation are given below:

1. F82H can withstand thermal loads twice as high as SS316 in the case of the same temperature gradient inside the specimen.
2. In case of 10000 cycles at a temperature difference of 600 K, there is a big difference in crack propagation, because the thermal expansion ratio of SS316 is twice higher than that of F82H.
3. From analytical simulations, the stress intensity factor of F82H is calculated to be one seventh of SS316. The qualitative tendency agrees with experimental results, however, there is still room to argue the small discrepancy between the experimental and the numerical result.
4. To reach a crack length of 30% of the specimen thickness, F82H can withstand 10 times more cycles than SS316. Concerning the thermal fatigue properties, there is no difference between F82H and commercial grade ferritic steel (9Cr-1Mo).

References

[1] K. Shiba et al., Properties of Low Activation Ferritic Steel F82H IEA Heat – Interim Report of IEA Round-robin Tests (1), Japan Atomic Energy Research Institute Technical Report JAERI-Tech. 97-038, 1997.
[2] K. Kikuchi et al., Fus. Eng. Des. 49&50 (2000) 229.
[3] S. Kimura et al., Fus. Eng. Des. 39&40 (1998) 569.
[4] MARC Analysis Research Corporation, MARC volume A, Theory and User Information Version K7, 1997.
[5] D. Broek, Elementary Engineering Fracture Mechanics, 4th Ed., Martinus Nijhoff, 1986.